PAPER

Check for updates

A biomass-derived metal-free catalyst doped with phosphorus for highly efficient and selective oxidation of furfural into maleic acid†

Huifa Zhang,[a] Shaolin Wang,[b] Huixian Zhang,[c] James H. Clark [ID][d] and Fahai Cao [ID] *[a]

The present work introduces an extremely simple and eco-friendly strategy for the highly selective synthesis of maleic acid (MA) *via* oxidation of renewable furfural using the abundant biomass-derived P–C-*T* catalyst. The P–C-*T* carbon catalyst was metal-free and prepared by the pyrolyzation of phytic acid, which is a ubiquitous natural molecule containing phosphorus. Extensive characterization was carried out to reveal the morphological and elemental properties of the synthesized P–C-*T* series. The effect of the annealing temperature of pyrolyzing phytic acid on the properties of the yielded P–C-*T* and subsequent catalytic performance was also explored. The catalytic oxidation of furfural to MA was carried out in the presence of H_2O_2 within an aqueous system. The reaction conditions including the catalyst loading, H_2O_2 concentration, reaction temperature and duration were further optimized. It was found that P–C-600 exhibited a remarkable catalytic activity for MA synthesis from furfural oxidation with a maximum yield of 76.3% achieved in water. The excellent catalytic performance of P–C-600 was attributed to its unique atomic layered structure and suitable acidity. P–C-600 could also be re-used for at least six runs without any obvious decrease in its catalytic performance. The intrinsic advantages of green synthesis, low cost, and excellent catalytic performance in the catalytic oxidation of furfural to MA suggested that P–C-600 would be a promising catalyst in future industrial applications for MA synthesis in a green manner.

Introduction

The exploration of renewable resources for sustainable production of chemicals and fuels is of urgent necessity and has attracted growing interest over the past decade due to the rapid depletion of fossil and other virgin resources. Biomass is a promising renewable carbon source,[1] and has the potential to be converted into chemicals and liquid transportation fuels at a large scale. It has been converted to many platform molecules, such as formic acid,[2] levulinic acid,[3] 2-furfuraldehyde (furfural),[4] 5-hydroxymethyl-2-furfural,[5] and lactic acid[6] that could be further used to synthesize a multitude of value-added products. Maleic acid (MA) is one of the value-added chemi-

cals derivable from biomass.[7] It is an important raw material in the chemical industry and has been extensively applied in multiple fields, such as medicine, plasticisers, copolymers, and agrochemicals.[7] Currently, MA is mainly produced from fossil fuels by the hydrolysis of maleic anhydride, and has high environmental burden and is limited more and more by fossil fuel depletion. Hence, the efficient synthesis of MA from renewable biomass based resources is of paramount importance.

In fact, many attempts have been devoted to the production of MA using biomass as the starting material. There are two main routes: the furfural[8–13] route and the HMF route.[14,15] Both routes are based on selective oxidation over various catalysts, either homogeneous or heterogeneous. Due to the problems of easy degradation and cross-polymerization, the synthesis of HMF from biomass at a large scale has not yet been successful.[16] Compared with HMF, furfural has been successfully produced from lignocellulose commercially, which paves the way for further MA synthesis.

For MA synthesis from furfural, both gas and liquid reaction systems have been reported. The liquid phase reaction system was preferred, since the reaction in the vapor phase can suffer from the drawbacks of low substrate concentration

[a] Engineering Research Centre of Large Scale Reactor Engineering and Technology of Ministry of Education, East China University of Science and Technology, Shanghai 200237, China. E-mail: fhcao@ecust.edu.cn

[b] Shanghai Key Laboratory of Green Chemistry and Chemical Processes, School of Chemistry and Molecular Engineering, East China Normal University, Shanghai 200062, China

[c] Sinopec North China E&P Company, Zhengzhou 450006, China

[d] Green Chemistry Centre of Excellence, University of York, York YO105DD, UK

†Electronic supplementary information (ESI) available. See DOI: 10.1039/d0gc04205f

and low MA yield because of the elevated reaction temperature. Various homogeneous and heterogeneous catalytic systems were then extensively explored for carrying out the reaction under aerobic conditions or in the presence of hydrogen peroxide in the liquid phase. Homogeneous systems are usually performed under mild conditions, but can suffer from considerable pollution. The first study of homogeneous systems can be traced back to the report by Yin *et al.* in 2011. In their work, the reaction was carried out in liquid media using phosphomolybdic acid as the catalyst and dioxygen as the oxidant.[17] A 49.2% yield of MA was achieved under the optimized reaction conditions with a 51.7% selectivity toward MA. In order to enhance the selectivity of MA, organic solvents were further introduced into the reaction systems by means of the reaction extraction method.[18] Later, other kinds of inorganic protic acids, such as sulfuric acid and hydrochloric acid,[19] were investigated for the catalytic oxidation of furfural to MA with hydrogen peroxide as the oxidant. Due to the extremely unstable character of furfural under acidic conditions, these homogeneous inorganic acid catalysts usually gave low MA yields. It was later demonstrated that C1–C4 organic acids can be catalytic systems as well as solvents.[12] The pK_a of organic acids was also shown to play a crucial role in the catalytic oxidation of furfural to MA with a 95% MA yield achieved in formic acid media. Adding an organic solvent to the reaction system is well acknowledged to enhance the yield of MA, but this is not consistent with the principles of green chemistry. What's more, the tedious procedures and high cost cannot be ignored for the recovery of homogeneous catalysts from the products after the reaction. Alternatively, heterogeneous catalysts were then developed to circumvent the above problems. Although metal catalysts, such as vanadium oxide-based,[17,20] titanium silicate-1 (TS-1),[8,11,21] copper phosphate[22] and Mo–V–O catalysts,[23] can give relatively high MA yields in the liquid phase oxidation of furfural, metal catalysts are also problematic due to potential leaching and deactivation during the reaction processes. In comparison, carbon-based materials are more promising as they have several distinct advantages, including large surface area, corrosion resistance, and the ability to tailor physicochemical and electronic properties. Sulfonated carbon materials, such as Amberlyst-15,[24] Nafion NR50,[24] Nafion SAC13[24] and SO3-GO,[25,26] were then developed to convert furfural into MA and SA, but such types of carbon catalysts containing sulfonic acid groups usually afforded a higher yield of SA over MA. Carbon materials doped with heteroatoms, such as nitrogen (N), boron (B), or phosphorus (P), are currently under intense investigation. A few pioneering trials were reported using heteroatom doped carbon catalysts to catalytically convert furfural to MA in the presence of hydrogen peroxide.[9,27] However, these N doped carbon catalysts are far from industrialization due to their performance.

A P doped carbon catalyst was proven to be an excellent catalyst in the oxidation of hydrocarbons and alcohols.[28–31] The lower electronegativity and larger diameter of P atoms endow P doped carbon materials with distinct features which could probably bring out distinct catalytic activities. What's

more, most P doping methods are accompanied by the formation of various P and O containing functional groups, such as phosphonate and phosphate groups,[31,32] making the catalysts acidic.[33,34] Hence, it was anticipated that P doped carbon materials could facilitate the reaction to selectively produce more MA from furfural. Considering the advantages of P doped carbon materials mentioned above and the fact that phytic acid is extremely abundant and easily available from legumes and cereals, the current work was designed and carried out to investigate the use of phytic acid as a starting material for the P–C catalyst for the catalytic oxidation of furfural to MA.

Herein, we report an extremely simple and eco-friendly strategy for the highly selective production of MA from furfural using a P-doped carbon catalyst derived from phytic acid. The catalysts were prepared by the pyrolysis of phytic acid at different annealing temperatures under an Ar atmosphere (P–C-*T*). Extensive characterization was carried out to reveal the morphological and elemental properties of the synthesized P–C-*T* series. The prepared P–C-*T* metal-free carbon catalysts were then used for MA synthesis in the presence of hydrogen peroxide at 333 K with pure water as the solvent. The reaction conditions of the catalytic oxidation of furfural to MA was further optimized when P–C-600, the best catalyst among the tested ones, was used. The reusability of P–C-600 was also evaluated to substantiate its practical application potential. This cheap, readily available, and environmentally friendly carbon catalyst is believed to be a promising catalyst for industrial applications of MA synthesis from a renewable resource in a green manner.

Materials and methods

Materials

Furfural (99%) and MA were of analytical grade and purchased from Aladdin Chemicals Co., Ltd (Shanghai, China). Fumaric acid was purchased from Sinopharm Chemical Reagent Co., Ltd (Shanghai, China). 50% (w/w) Phytic acid aqueous solution was purchased from Tianjin Guangfu Chemical Industry (Tianjin, China). Hydrogen peroxide aqueous solution 30% (w/w) and other main reagents used in the study were purchased from Shanghai Titan Scientific Co., Ltd (Shanghai, China) and they were analytically pure. All chemicals except furfural were used as received without further purification. Furfural was purified by distillation before use.

Catalyst preparation

Preparation of the P doped carbon catalyst. The P–C-*T* carbon catalyst was synthesized according to the following procedures. 10 g of 50% phytic acid solution was first subjected to hydrothermal treatment in an oven at 120 °C for 24 h. The semi-solidified mixture was then collected and calcined in a muffle furnace at different temperatures (500, 600, 700 and 800 °C) for 4 h under an argon atmosphere with a heating rate of 3 °C min^{-1}. The obtained black granular materials were

ground to powder and termed P–C-*T*, where *T* represented the annealing temperature.

Catalyst characterization. The overall morphologies of P–C-*T* carbon catalysts were analyzed using a Hitachi S-4800 scanning electron microscope (SEM) instrument operated at an accelerating voltage of 3.0 kV. The microstructures of the P–C-*T* carbon catalysts were tested on a Tecnai G2 F30 transmission electron microscope (TEM) instrument operating at an accelerating voltage of 200 kV. TEM samples were prepared by dissolving the P–C-*T* catalyst in ethanol and were transferred onto a copper TEM grid coated with a holey support film. The solvent of the dropped sample was evaporated in air at room temperature before testing. The phase composition of the synthesized samples was determined using a Bruker D8 Advanced XRD (X-ray diffractometer) in the 2θ range between 10 and 80° with Cu-kα (λ = 1.541 Å) operating at room temperature at a scanning rate of 0.016° s^{-1}. To analyze the physical surface characteristics of the synthesized carbon catalysts, N$_2$ adsorption–desorption measurements were carried out using an ASAP 2020 (Micromeritics). The samples were degassed in a vacuum at a temperature of 350 °C for 6 h to remove impurities prior to the measurements. Surface areas were estimated using the Brunauer–Emmett–Teller (BET) model. Pore size distribution of carbon samples was calculated *via* the Barrett–Joyner–Halenda (BJH) method. Raman spectra of the samples were recorded using a laser with an excitation wavelength of 785 nm at room temperature using the Horiba Jobin Yvon LabRAM HR800 Raman spectrometer. The elemental composition and bonding information of carbon catalysts was determined by X-ray photoelectron spectroscopy (XPS, PHI-5702). Generally, the charge-up shift of all samples was corrected by the standard binding energy peak of C 1s (284.6 eV). Elemental mapping was carried out using STEM-EDS. In order to study the acidic properties of the prepared carbon catalysts, temperature programmed desorption of ammonia (NH$_3$-TPD) of samples was carried out on a Micromeritics ChemiSorb 2920 equipped with a TC detector (TCD). Before carrying out the TPD, samples of 100 mg were first thermally treated *in situ* at 300 °C for 2 h in flowing helium to remove the gases physisorbed on the sample surface. NH$_3$ was chemisorbed on the catalyst at 50 °C for 1 h and then desorption of ammonia was carried out under a flow rate of 40 ml min^{-1} of helium from 50 to 700 °C at a linear heating rate of 10 °C min^{-1}. Desorbed NH$_3$ was measured quantitatively using the TCD detector. FT-IR pyridine adsorption technique was used to investigate the Lewis and Brønsted acidic sites of the catalysts. Pyridine infrared spectroscopy (Py-IR) was recorded on a Bruker Vertex 70. Self-supporting disks (6.5 mm diameter, 10 mg) of the samples were prepared applying 6 ton pressure. Prior to the measurements, the samples were dehydrated by heating at 400 °C for 3 h under vacuum. After cooling down, pyridine adsorption was conducted in a saturated pyridine atmosphere at room temperature for 5 h. Subsequent pyridine desorption was carried out at different temperatures for 30 min and the infrared spectrum was recorded. The concentration of Brønsted and Lewis acidic sites in the carbon samples was esti-

mated by using integrated molar extinction coefficients.[35] The solid state ^{31}P MAS NMR experiments were carried out on a Bruker Avance AV 300 spectrometer at a Larmor frequency of 600 MHz using a single pulse with a high power decoupling sequence. Inductively coupled plasma mass spectrometry (ICP-MS) measurement was performed using an Agilent ICP-MS 4500 instrument to detect the leaching of P to the reaction solution.

Catalytic reaction. The catalytic oxidation of furfural was carried out in a 70 ml Teflon-lined stainless steel reactor. The reactor was integrated with an oil bath and a magnetic stirrer, which could be used to control the temperature and stirring rates of the reactor precisely. In a typical reaction, the procedure for furfural oxidation was as follows: 2.5 mmol furfural, 1.96 g 30 wt% H$_2$O$_2$ (H$_2$O$_2$, 20 mmol, determined by iodometric titration), 0.15 g P–C-*T* carbon catalyst and 5 ml water were successively added into the above reactor. After sealing the valve, the sealed reactor was heated using the oil bath to the specified temperature within a certain time duration. The reaction was carried out under vigorous stirring and maintained at the reaction temperature for a specific duration. After the reaction, the mixture was cooled to room temperature with iced water. The products were collected and separated using a filter. Quantitative analysis of the product was performed using HPLC equipped with an XDB-C18 reversed phase column and a UV detector (mobile phase 5 : 95 ratio of acetonitrile: 0.01% phosphoric acid, flow rate 0.6 mL min^{-1}, 240 nm).

Results and discussion

Characterization of carbon catalysts

In this study, a renewable biomass-derived molecule, phytic acid, a unique natural substance containing phosphorus ubiquitously found in legumes and grains, was chosen as the starting material of P–C-*T* carbon catalysts. Phytic acid is a sixfold dihydrogen phosphate ester of inositol containing the same level of C and P in one molecule, thus guaranteeing a uniform P doping in the fabricated carbon catalysts. The synthesis process of P–C-*T* is illustrated in Scheme 1. The as-received phytic acid solution (50 wt%) was used directly without further purification. After being heated in an oven at 120 °C for 24 h, the semi-solidified mixture was annealed at different temperatures for 4 h under an argon atmosphere. The obtained black carbon residues were then ground to powder and termed P–C-*T* catalyst.
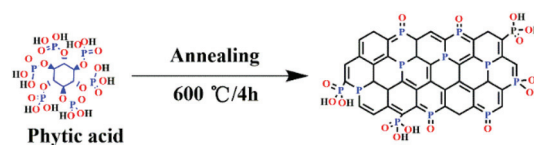
Scheme 1 Conversion route of phytic acid to P–C-*T*.

All of the P–C-T carbon samples prepared from phytic acid precursors exhibited an aggregated morphology with particles of a size of several micrometers according to the images shown in Fig. 1 (left), while the microporous structure of them was shown by the TEM images (right column of Fig. 1). The as-prepared P–C-T catalysts possessed a lacunaris graphene-like structure with an obvious thickness sheet. It seemed that the morphology of the P–C-T catalysts was affected by the annealing temperature. More pores could be developed with the increase in the pyrolysis temperature, resulting in more defects evolved in the carbon materials. In addition, it was also clear that from the TEM images that the thickness of the materials became thin obviously with the increase of pyrolysis temperature. High-resolution TEM analysis was further carried out to reveal the texture structure of the P–C-600 catalyst, and abundant irregular pores could thus be clearly observed (Fig. 2). The corresponding STEM-EDS elemental mapping images of the P–C-600 catalyst are shown in Fig. 2, and it could then be confirmed that P element was uniformly incorporated into the graphene-like carbon framework.

Since it is well known that specific surface area and pore size distribution are two important features of catalysts, especially the carbon materials for catalytic performance, BET measurement of the as-prepared P–C-T was performed. As shown in Fig. 3a, a typical type-IV isotherm curve with a H4 hysteresis loop at low-relative and medium pressure was observed, indicating the coexistence of both mesoporous and microporous structures in all as-synthesized P–C-T catalysts. These results were consistent with the TEM images. The respective surface areas were calculated *via* the (BET) method,
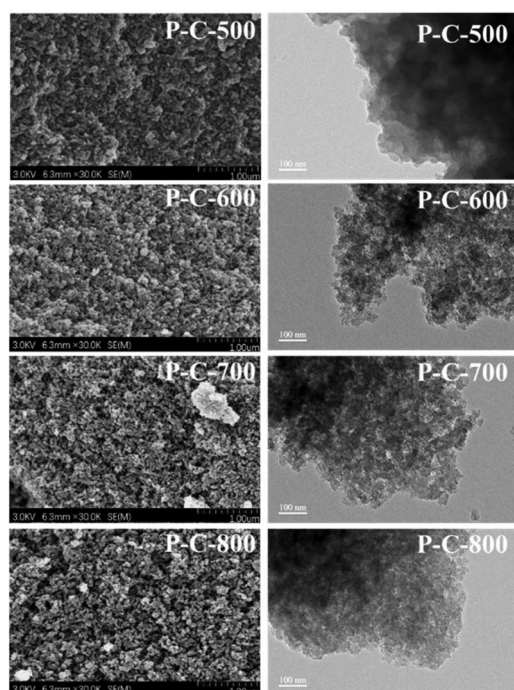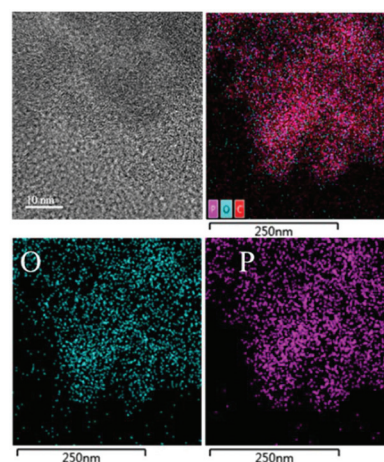

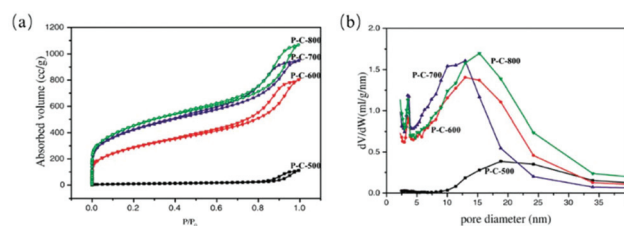**Fig. 2** High-resolution TEM image and elemental mapping of P–C-600.

Fig. 3 (a) N$_2$ adsorption/desorption isotherms and (b) BJH pore size distribution curves of P–C-T.

as shown in Table 1. P–C-500, P–C-600, P–C-700 and P–C-800 had the specific surface areas of 33.7 m^2 g^{-1}, 1038.6 m^2 g^{-1}, 1521.6 m^2 g^{-1} and 1637.4 m^2 g^{-1}, respectively (Table 1). The surface areas of the P–C-T catalysts were greatly affected by the pyrolysis temperature. The higher the annealing temperature, the higher the specific surface area of the catalyst sample was. It was interesting to notice that the pore size of all samples could be divided into two types: micropores with diameters of 0.02–0.8 nm and mesopores with diameters of 0.2–3.5 nm. Both the microporous and mesoporous pore size also greatly increased with an increase of the pyrolysis temperature. A significant porosity enhancement was obtained when the annealing temperature increased to 500 °C and higher. It could then be ascertained that the morphological features of the P–C-T carbon catalysts largely depended on the treatment temperature based on the above results.

Table 1 Structural properties of P–C-T

Entry	Surface area (m^2 g^{-1}) meso/micro		Pore size (nm) meso/micro		Pore volume (ml g^{-1}) meso/micro	
P–C-500	33.7	32.5	0.2	0.02	18.8	0.86
P–C-600	1038.6	387.6	0.92	0.17	3.5	1.02
P–C-700	1521.6	774	0.95	0.35	3.5	0.48
P–C-800	1637.4	898	3.5	0.84	1.09	0.41

Fig. 1 SEM (left) and TEM (right) images of the synthesized P–C-T.

The X-ray diffraction patterns of the prepared carbon samples are shown in Fig. 4. Two peaks at around 24.5 degree and 44 degree could be evidently observed in the XRD patterns of P–C-600, P–C-700, and P–C-800, whereas only one peak at 24.5 degree could be distinguished pertaining to P–C-500. The dominant and broad peak centered at 24.5 was corresponding to the (002) reflection of graphite, suggesting that the synthesized samples were highly amorphous with a typical turbostratic graphite structure.[36,37] The peak centered at 44 degree reflected the size of the aromatic layers. The intensity of the peak at around 44 degree enhanced with the annealing temperature, suggesting the formation of intralayer condensation in the graphite layers in the catalysts synthesized under a higher pyrolysis temperature.

Raman spectroscopy was further used to investigate the doping effect of graphene. The Raman spectra of all samples (Fig. 5) displayed a typical D band and a G band peak appeared at 1330 and 1600 cm^{-1}, respectively. The relative strength of the D-band is a reflection of the degree of the sp^3 defect sites in the graphite structure and the G-band is associated with the sp^2 carbon networks. The relative intensity ratio of I_D/I_G ratio is typically used to evaluate the level of defects and heteroatom doping. The I_D/I_G ratios of P–C-500, P–C-600, P–C-700 and P–C-800 were 2.55, 2.73, 1.93 and 1.91, respectively. The results indicate that pyrolysis was a co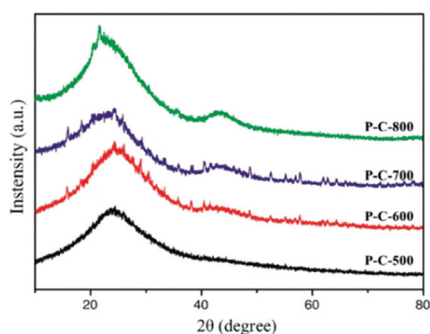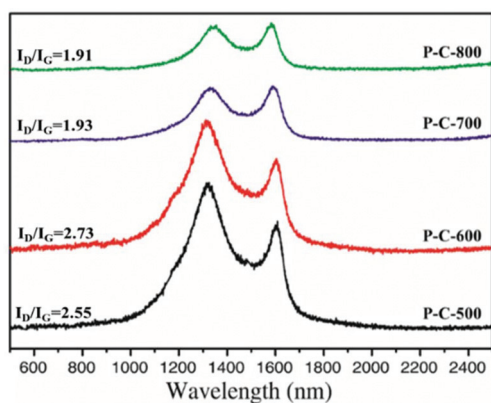mplicated process. More defects instead of graphitization might be evolved in the carbon structures under a high pyrolysis temperature, thus resulting in an increase in I_D/I_G. At the same time, less P heteroatoms could be grafted into the carbon lattice as more phosphorus atoms would be peeled off from the carbon lattice. Accounting to the fact that the defect level of carbon materials and the degree of P heteroatoms doped on the carbon catalyst both determined the catalytic activity, the balance of the defect level and P doping degree on the current carbon catalyst should be optimized to favor the catalysis.

In order to quantitatively determine the elemental composition and valence states of elements in the P–C-T, XPS was carried out and the results are shown in Fig. 6. It was noted that four predominant peaks at 284.6 eV, 532 eV, 193 eV, and 133 eV corresponding to C 1s, O 1s, P 2s, and P 2p, respectively, appeared in the XPS spectra of all P–C-T carbon materials, confirming the successful synthesis of carbon materials doped with P by annealing the biomass derived phytic acid containing phosphorus under an elevated temperature. This was consistent with the above EDS mapping results. The relative percentages of various atoms of the P–C-T catalysts calculated from the XPS spectra are summarized in Table 2. It should be noted that the atomic relative composition of P decreased significantly with the increase in the annealing temperature, but with a concomitant increase in the percentage of C atoms. A similar trend was observed for the element O. The decrease of P and O atomic concentration with the increase in the pyrolysis temperature could be attributed to the fact that the heteroatoms could be desquamated from the
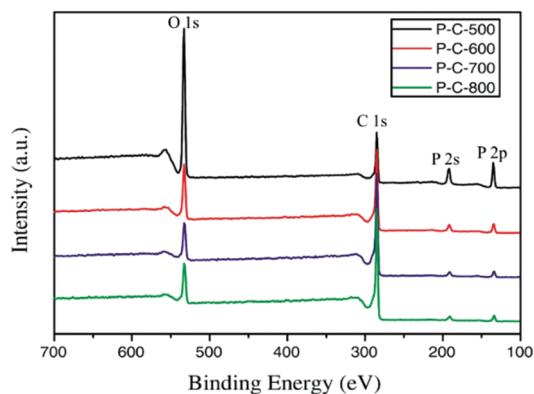

Fig. 4 X-ray diffraction patterns of P–C-T.

Fig. 5 Raman spectra of P–C-T.

Fig. 6 XPS scan spectra of P–C-T.

Table 2 XPS analysis on the element contents of P–C-T

Entry	Catalyst	Total (%)			Calculated (%)	
		C (at%)	P (at%)	O (at%)	P–C (at%)	P–O (at%)
1	P–C-500	38.17	13.59	48.24	0.38	13.21
2	P–C-600	72.82	6.37	20.8	0.19	6.18
3	P–C-700	82.06	3.69	14.25	0.15	3.54
4	P–C-800	82.86	3.58	13.56	0.2	3.38

doped carbon materials under a high pyrolysis temperature. Considering that the acidity strength of the catalyst is directly related to the phosphorus content,[34,38] a high treating temperature may lead to the decrease of the acidity of the catalyst. The C 1s peak in the high resolution XPS was deconvoluted into three components attributed to O–C=O (289.5 eV), C–C (284.6 eV), and C–P (285.9 eV) bonds, respectively (Fig. S1†). The deconvolution of the high-resolution P 2p band described two types of P species at 132.6 eV and 134.2 eV, corresponding to the P–C and P–O groups, respectively (Fig. 7). The formation of the P–C bond under an elevated temperature indicated that P atoms were incorporated into the carbon lattice at a higher carbonization. Furthermore, the relative peak area ratio of P species was greatly affected by the pyrolysis temperature. The relative peak area ratio of P–C gradually increased with the increase in the pyrolysis temperature, whereas the one of P–O decreased in turn. A similar phenomenon has been reported by many research studies.[39,40] This may be due to the fact that the dissociation energy of the P–C bond is higher than that of the P–O bond.[41] The polarity of the P–C bond is opposite to that of the N–C bond.[31] The lower electronegativity of P atoms than the C atoms makes the P atoms in the P–C bond with positively charge, which may result in its Lewis acidity in the catalyst.[42] The Brønsted acidity might be originated from the surface P–O groups (phosphonate and phosphate groups).[39,43,44] In summary, it was reasonable to suggest that the treating temperature not only greatly affected the acidity strength of the catalyst, but also the types of acidic sites. The pronounced O 1s spectrum was fitted into three sub-peaks, C/P=O (531.4 ± 0.1 eV), C/P–O–C (532.5 ± 0.1 eV) and C/P-OH (533.5 ± 0.1 eV), respectively (Fig. 7). Considering all the above results, the successful synthesis of P–C catalysts can be ascertained.

As mentioned in the introduction, the acid of this P doped carbon material might play a determining role in the catalytic oxidation of furfural to MA. The acid amount and strength of the as-synthesized P–C-T catalysts was then analyzed by a NH$_3$-
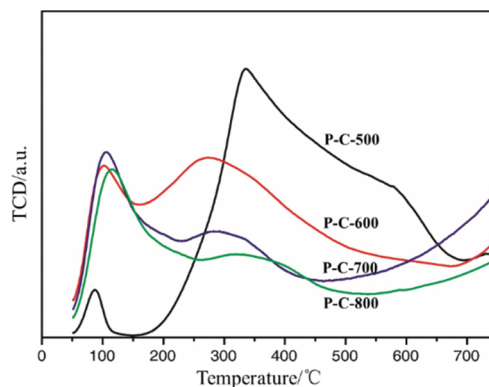

Fig. 8 NH$_3$-TPD profiles of P–C-T.

TPD method and the results are shown in Fig. 8. All of the synthesized samples exhibited two broad NH$_3$ desorption peaks at around 100 °C and 300 °C, respectively. The former was attributed to weak acidic sites, while the latter was usually considered to be the medium acid sites.[45] It could be seen from Fig. 8 that P–C-500 and P–C-600 owned more medium-strength acid sites than P–C-700 and P–C-800. In addition, it is worth noting that the total acid amounts introduced to carbon decreased when the pyrolysis temperature increased from 500 to 800 °C. This might be attributed to the fact that the heteroatoms grafted on carbon could be destroyed under an elevated temperature, thus resulting in less phosphonate and phosphate groups in the P–C-T catalysts.

To further investigate the types of acidic sites, the surface acidity was studied by pyridine adsorption experiments. The IR spectra of adsorbed pyridine over P–C-600 at different temperatures are shown in Fig. 9. Three adsorption peaks at about 1540 cm^{-1}, 1490 cm^{-1} and 1450 cm^{-1}, corresponding to the adsorption of pyridine at the Brønsted acidic sites (B), Brønsted and Lewis acidic sites (B + L) and Lewis acidic sites (L), respectively, were clearly observed in all the samples. However, as compared to P–C-500 (Fig. S2†), the major acid sites were Brønsted acid sites, while most of the acid sites of
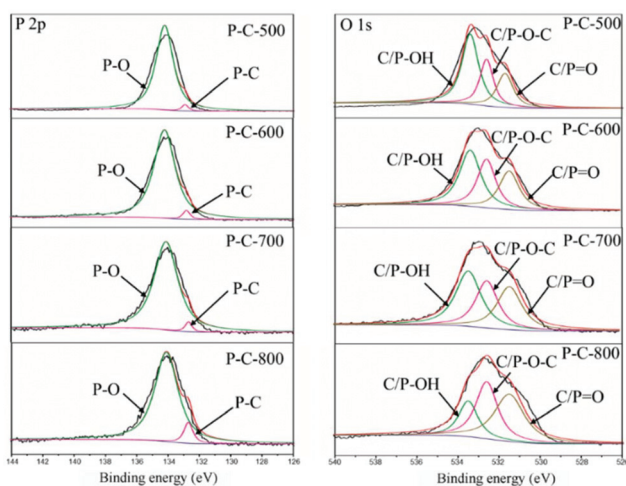

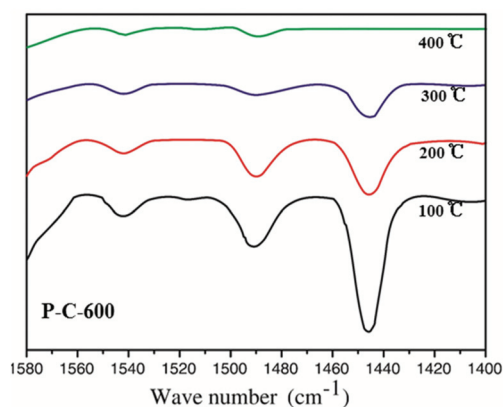**Fig. 7** XPS high-resolution P 2p (left) and O 1s (right) spectra of P–C-T.

Fig. 9 Pyridine-FTIR spectra of P–C-600 obtained after evacuation at different temperatures.

the other three carbon catalysts were Lewis acid sites. This could be attributed to the fact that more relative P–C bonds were evolved under a higher treating temperature leading to the generation of relatively higher Lewis acidity sites. What's more, the band of the three obvious peaks of the four carbon catalysts decreased dramatically with the increase in the desorption temperature, suggesting that almost all kinds of acid sites on these four catalysts are relatively weak. These results were coincident with the NH_3-TPD results. The above results revealed that the increase in the pyrolysis temperature can reduce the strength of the strong acid sites of the obtained catalysts. The quantitative results of the acid sites obtained by the integral peak areas are summarized in Table S1.† Quantification of the medium and strong acid sites was performed using the data obtained from the spectra of the adsorbed pyridine according to the method reported.[35] As shown, the medium acidic sites of P–C-500 and P–C-600 were more than their weak acidic sites and strong acidic sites, respectively. Total acid amounts decreased gradually with increasing the carbonization temperature from 500 to 800 °C. This was consistent with the NH_3-TPD results. It is worth noting that the total Lewis acid sites of the P–C-T reached a maximum at around 600 °C. This might be due to the fact that more P atoms were incorporated into the carbon lattice under a higher treating temperature above 600 °C. Further increasing the pyrolysis temperature above 600 °C to 800 °C would destroy the P atoms in the carbon structure, resulting in a decrease in the total Lewis acid sites. Considering that the acidity of the catalysts might be significantly beneficial for the oxidation of furfural to MA, P–C-500 and P–C-600 obtained under a lower annealing temperature might have more active sites.

The chemical environment of the P atoms in the synthesized material had been investigated with solid state NMR and the results are shown in Fig. 10. ^{31}P NMR spectra of P–C-500 showed four dominant signals centered at 31 ppm, −11 ppm, −25 ppm, and at −42 ppm which corresponded to
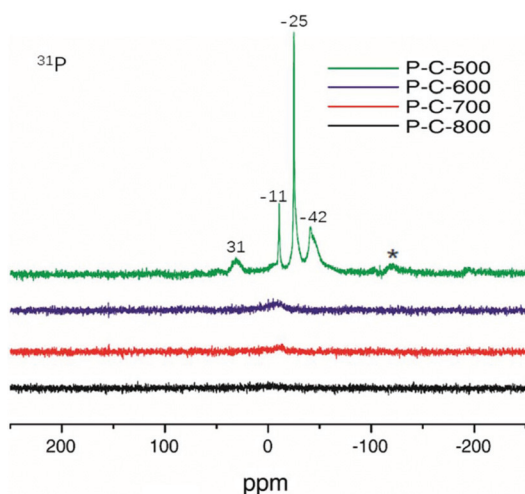
four different P–O moieties.[46–48] The ^{31}P NMR spectra of other three carbon catalysts exhibited different behaviours with the P–C-500 catalyst. Almost no obvious peaks could be observed in the ^{31}P NMR spectra of the three catalysts. Furthermore, the peak at around −11 ppm gradually decreased with increasing pyrolysis temperature and vanished at 800 °C. All these results indicated that the P–O bond gradually decreased with the increase of the catalyst calcination temperature, which was in agreement with the XPS results. ^{31}P NMR spectra of the P–C species were barely detected. This might be attributed to two reasons. Small amount of P atoms were grafted onto the carbon lattice leading the signals lower than the noise. On the other hand, ^{31}P NMR spectra of the P–C bond are usually relatively broad peaks, which are difficult to distinguish.

Catalytic performance

Catalytic oxidation of furfural into MA over various catalysts. The catalytic activity of the as-synthesized P–C-T catalysts was evaluated by the oxidation of furfural in the presence of H_2O_2 and the results are presented in Table 3. For comparison, carbon derived from glucose was also investigated for this reaction. As shown in Table 3, when the oxidation reaction was conducted without any catalysts, only 30.1% of furfural could be converted with a trace yield of maleic acid (Table 3, entry 1), which confirmed the necessity of catalysts for this reaction. The low yield of MA could be attributed to the fact that furfural was highly prone to non-selective polymerization, forming furanic resins. The conversion of furfural and the selectivity of MA over the C-600 catalyst was 51.5% and 26.0%, respectively (Table 3, entry 2). It was interesting to notice that the furfural conversion and MA selection was tremendously enhanced upon the application of current P–C-T as the catalysts. As shown in Table 3 (entries 3–6), the highest furfural conversion was obtained when P–C-500 was used, while the highest MA yield (62%) was achieved with P–C-600. The furfural conversion decreased in an order of P–C-500, P–C-600, P–C-700 and P–C-800 with the same loading of catalysts, whereas the selectivity of MA exhibited a different phenomenon, suggesting that the catalytic activity of P–C-T catalysts was pronouncedly affected by the annealing temperature. It was worth noting that the conversion of furfural was positively related to the total number of acid sites, while the selectivity of MA was positively related to the amount of Lewis acid sites. P–C-600 could

Fig. 10 ^{31}P-NMR spectra of P−C-T.

Table 3 Oxidation of furfural to MA over various catalysts in the presence of H_2O_2

Entry	Catalyst	Catalyst loading (mg)	Furfural Con. (%)	MA yield (%)	MA Sel. (%)
1	Blank	0	30.1	3.3	11
2	C-600	100	51.5	13.4	26
3	P–C-500	100	96.6	42.9	44.4
4	P–C-600	100	89.9	62	69
5	P–C-700	100	72.5	42.8	59
6	P–C-800	100	69.3	39.5	57
7	P–C-1200	100	60.6	18.5	30.6

offer the best catalytic performance for the selective oxidation of furfural to MA (entry 4) among all synthesized P–C-*T* catalysts with an 89.9% conversion of furfural and a 69.0% selectivity of MA. According to the NH_3-TPD and Py-IR results, it was noted that the absolute amount and relative proportion of Lewis acid sites of P–C-600 were the highest among all the carbon catalysts synthesized. Therefore, it was speculated that the Lewis acid sites could be the active sites for the oxidation of furfural into MA in the presence of H_2O_2, rather than the total amount of acid sites or Brønsted acid sites. For comparison, P–C-1200 catalyst doped with less P was also tested in parallel under the same reaction conditions. A 18.5% yield of MA was obtained over the P–C-1200 catalyst, which was slightly higher than the yield obtained over the C-600 catalyst. Moreover, only 1.78% P (at%) has been detected by XPS in the P–C-1200 catalyst, much lower than the P content in the other four P carbon materials. These results further confirmed that the acid sites were the key active sites in the catalytic oxidation of furfural into maleic acid. Hence, P–C-600 was chosen as the catalyst in the following experiments for further optimization of this oxidation reaction if not otherwise indicated.

Effects of catalyst dosage on the catalytic oxidation of furfural into MA over P–C-600. To further optimize the reaction conditions, the influence of catalyst dosage on the catalytic performance with varying amounts from 0.05 to 0.3 g was investigated within the same reaction system. The correlation between catalyst dosage and furfural conversion as well as MA selectivity/yield is shown in Fig. 11. As expected, the furfural conversion exhibited a positive correlation with the loading of P–C-600 within the tested amount range, whereas the selectivity to MA increased first with the increase in the catalyst amount and then decreased, suggesting that the active sites of catalysts could promote the formation of MA only to a certain extent. When the loading of the catalyst increased from 0.05 to 0.15 g, the selectivity to MA increased from 59.0 to 74.5%. With the further increase from 0.15 to 0.3 g, the selectivity of MA decreased from 74.5% to 66.0%. This might be partly attributed to the unstable characteristics of furfural, especially in the presence of an acid catalyst. Since the maximum yield of MA (69.1%) was achieved with 0.15 g P–C-600 catalyst, the fol-

lowing experiments were fixed at this dosage if not otherwise indicated.

Effects of the H_2O_2 amount on the catalytic oxidation of furfural into MA over P–C-600. The effect of H_2O_2 concentration within the reaction system on the catalytic oxidation of furfural to MA was also examined over P–C-600 at 60 °C for 6 h. The correlation of furfural conversion and MA selectivity with the H_2O_2 concentration from 10–30 mmol is thereby shown in Fig. 12. It was shown that the H_2O_2 amount was also crucial for the reaction to proceed. Remarkably, within the current concentration range, the larger the H_2O_2 concentration, the higher the furfural conversion. Of note, when the reaction was performed without H_2O_2 addition, the conversion of furfural could be neglected. The MA yield could be increased from 41.9% to 69.1% when the H_2O_2 concentration was increased from 10 to 20 mmol. However, further increase in H_2O_2 concentration to 30 mm only showed a negligible improvement on the MA yield. Hence, it could be confirmed that H_2O_2 played an important role in the oxidation of furfural to MA and the optimum H_2O_2/furfural mol ratio was approximately 8 (20 mmol H_2O_2), which was then fixed in the following studies.

Effects of the reaction temperature on the catalytic oxidation of furfural into MA over P–C-600. The effect of the reaction temperature on the catalytic oxidation of furfural into MA over P–C-600 was also explored and the results are shown in Fig. 13. It could be seen that both the conversion of furfural and the selectivity of MA were sensitive to the reaction temperature. Although the conversion of furfural increased with the increase in the reaction temperature, the MA selectivity and yield reached the maximum (74.5% and 69.1%) at 60 °C. The further increase in the reaction temperature from 60 to 80 °C did not result in any improvement in the MA yield. This could be ascribed to two aspects. Furfural was very unstable under a high temperature, which could result in the polymerization of furfural. On the other hand, a high reaction temperature could facilitate the decomposition of peroxides, which were crucial for the oxidation of furfural to MA. Accordingly, the optimal
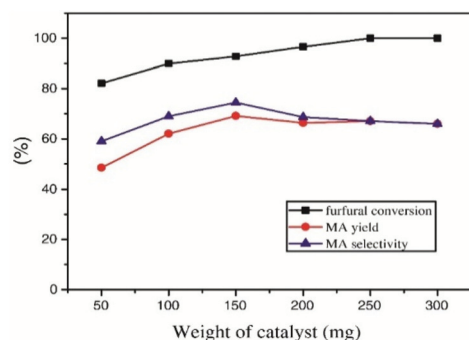

Fig. 11 Effects of the P–C-600 loading amount on the oxidation of furfural into MA. Reaction conditions: 2.5 mmol of furfural, 5 ml H_2O, 20 mmol H_2O_2, 60 °C, 6 h.
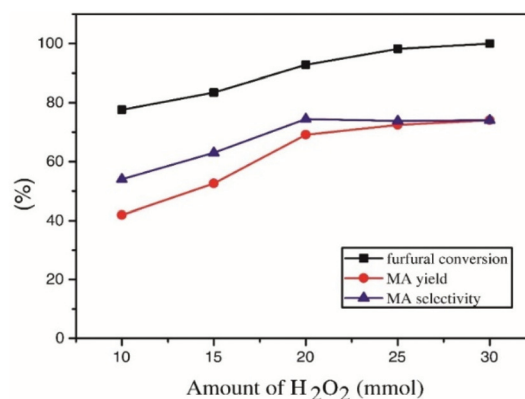

Fig. 12 Effects of the H_2O_2 amount on the oxidation of furfural into MA. Reaction conditions: 2.5 mmol of furfural, 5 ml H_2O, 0.15 g catalyst, 60 °C, 6 h.
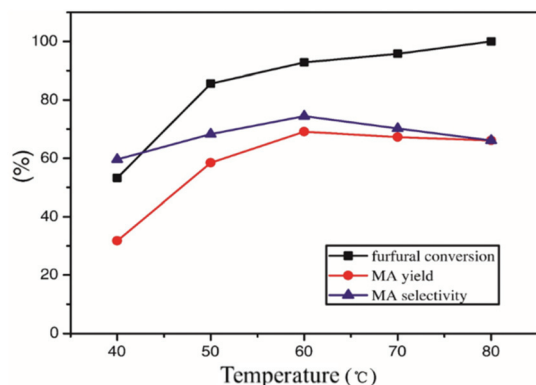
Fig. 13 Effects of the reaction temperature on the oxidation of furfural into MA. Reaction conditions: 2.5 mmol of furfural, 5 ml H_2O, 0.1 g catalyst, 20 mmol H_2O_2, 60 °C, 6 h.

reaction temperature for P–C-600 catalytic oxidation of furfural to MA was 60 °C based on the above compromised effects.

Effects of the reaction duration on the catalytic oxidation of furfural into MA over P–C-600. The effect of the reaction duration was also studied in order to obtain the maximum MA yield in the current reaction system. The corresponding correlation of the time courses with the furfural conversion and MA yield over P–C-600 is shown in Fig. 14. It was shown that the conversion of furfural had a positive relation to the reaction time. The oxidation of furfural was quite fast at the beginning of the reaction, and it took only around 2 h to reach the furfural conversion of 82.5%. The further increase in the reaction duration to 6 h resulted in the furfural conversion of 92.8%. It seemed that the catalyst was highly active for this reaction. Unlike the trend of furfural conversion, the yield of MA increased gradually and reached a maximum at 10 h (76.3%) with a concomitant yield of furoic acid smaller than 2% at all reaction durations. Further prolonging the reaction duration did not result in any increase in the yield of MA. It was indicated from these results that MA was stable in this reaction system. This might be attributed to the formation of some
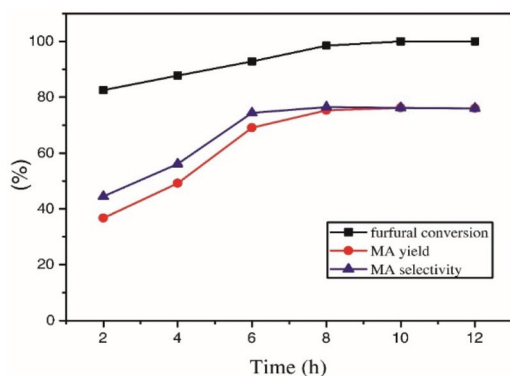
intermediate product during the reaction, which increased at the beginning and reached a maximum at 4 h, then decreased rapidly beyond 4 h, while the selectivity of MA increased accordingly.

To date, only several metal-free heterogeneous catalysts have been investigated for this reaction. A comparison of P–C-600 catalyst *vs.* metal-free heterogeneous catalysts reported previously for the synthesis of MA from furfural is shown in Table 4. It was evident that the P–C-600 catalysts afforded the highest MA yield. Sulfonated carbon catalysts usually afforded a higher yield of SA with a low yield of MA. Compared with the sulfonated carbon catalysts, the NC-900 catalyst could afford a relatively high MA yield. However, the preparation process of the NC-900 catalyst was quite complex. Thus, the P–C-600 catalyst exhibited a remarkable catalytic performance with a 76.3% MA yield, which indicated good efficiency of the catalyst for the synthesis of MA.

Reusability of P–C-600. In addition to the catalytic performance of P–C-600 for the oxidation of furfural to MA, the reusability of catalysts was also an important issue in practical applications. Therefore, the reusability tests of P–C-600 were performed by successive reuses at 60 °C for 10 h. After each run, the catalyst was recovered simply by centrifugation and thoroughly washed with 75% ethyl alcohol and dried overnight at 120 °C in an air oven. In order to avoid the impact of catalyst loss, each reuse was scaled down. The test results are presented in Fig. 15. It could be seen that the yield of MA remained almost constant (76%) even after four successive runs. A minor drop was noticed in the sixth cycle. However, when the cycles exceeded 7 runs, the catalyst showed a continuous decrease of activity.

The decrease of activity could be ascribed to the deposition of humin formed *via* the polymerization of furfural on the surface of P–C-600 during the reaction.

To further investigate the reasons for the decrease in the activity, P in the reaction solution had been detected by ICP. No P had been detected in the reaction solution, indicating that the acid sites were not leached into the solution. Moreover, the spent P–C-600 catalyst (after 8 runs) was characterized by TEM, BET (Fig. 16) and XPS (Fig. S4 and S5†). It was

Fig. 14 Effects of the reaction time on the oxidation of furfural into MA. Reaction conditions: 2.5 mmol of furfural, 5 ml H_2O, 0.15 g catalyst, 20 mmol H_2O_2, 60 °C.

Table 4 The comparison of catalytic activity and selectivity of different metal-free heterogeneous catalysts for the catalytic oxidation of furfural to MA

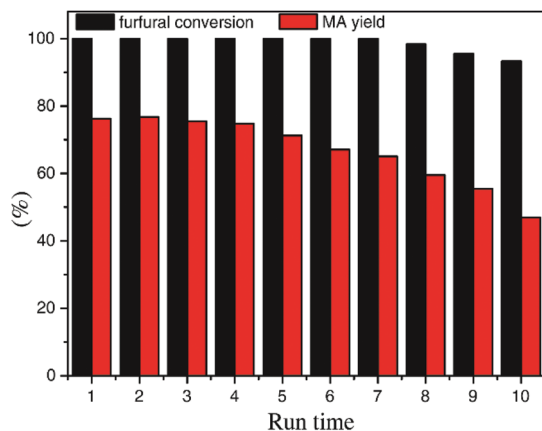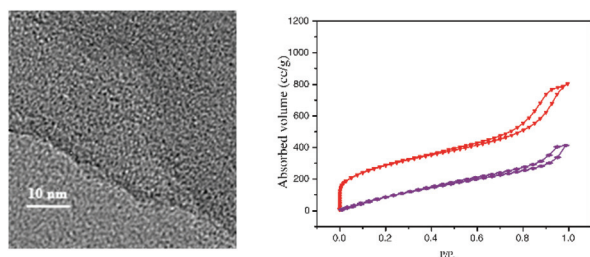| Entry	Catalyst	Reaction conditions	MA yield (%)	MA Sel. (%)	Ref.
1	NC-900	80 °C, 5 h	61.0	61.0	27
2	Amberlyst-15	80 °C, 5 h	16.0	16.3	27
3	g-C_3N_4	100 °C, 3 h	16.8	16.82	9
4	Nafion NR50	70 °C, 24 h	11.3	11.3	24
5	Nafion SAC13	70 °C, 24 h	9.5	9.5	24
6	SO_3H-carbocatalysts	80 °C, 1 h	34.3	34.3	26
7	SO_3H/GO	70 °C, 24 h	1.2	1.5	25
8	P–C-600	60 °C, 6 h	69.1	74.5	This work
9	P–C-600	60 °C, 10 h	76.3	76.3	This work

Fig. 15 Cycle usage of P–C-600.

Fig. 16 High-resolution TEM image (left) and N_2 adsorption/desorption isotherms (right) of the spent P–C-600. Reaction conditions: 2.5 mmol of furfural, 5 ml H_2O, 0.15 g catalyst, 20 mmol H_2O_2, 6 h.

clear that there was no obvious difference between the fresh P-C-600 and the spent P–C-600 catalyst from the TEM and XPS results. However, the BET analysis results indicated that the surface area of the spent P–C-600 carbon catalyst (382.6 m² g⁻¹) was much lower than that of the fresh P–C-600 catalyst (1038.6 m² g⁻¹). This might be attributed to humin deposited on the active sites by the polymerization of furfural on the surface of the catalyst during the reaction process. This deposition decreased the exposure of the acid active sites, thus resulting in a decrease in the activity of the catalyst. Although the mechanism of humin deposition is still unknown, some attempts have been made to remove the deposition of humins on the catalyst.[49] For example, low molecular weight humins formed at a low temperature can be removed by washing with an organic solvent. Moreover, humins can also be removed by hydrogenation.[50] It was thus speculated that the humins generated in this process might be partially or completely removed by hydrogenation or washing with an organic solvent.

Reaction pathway for MA from furfural. Although the reaction pathway of the acid-catalyzed oxidation of furfural to MA in the presence of H_2O_2 was still under debate, four types of reaction paths have been proposed, as shown in Scheme S1.†
In route 1[10,51] and route 2,[52] furoic acid and furan are the two oxidation intermediates during MA formation from furfural. A Baeyer–Villiger oxidation is accompanied in path 3[10] and path
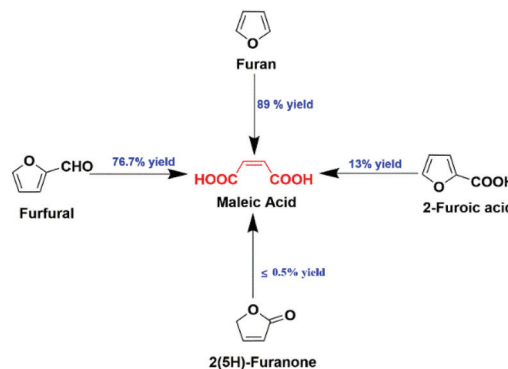

Fig. 17 Oxidation of various substituted furan compounds under optimized reaction conditions: substrate (1 mmol), formic acid (4 ml), 31% H_2O_2 (1 ml), 100 °C, 4 h.

4.[12,19,24] 2(5H)-furanone is an important intermediate associated with the formation of MA from furfural in path 4, while Z-4-oxopent-2-enedial is reported to be one of the intermediates in pathway 3. To determine the specific reaction pathway for the acid-catalyzed H_2O_2 oxidation of furfural to MA over the current P–C-600, three plausible intermediates, furoic acid, furan and 2(5H)-furanone were tried under the optimized oxidation conditions. As shown in Fig. 17, the yield of MA obtained from 2(5H)-furanone was trace and only a 5% conversion of 2(5H)-furanone was converted. However, with furan and furoic acid, the yield of MA was 89% and 13%, respectively. In spite of the fact that furan can offer an 89% yield of MA, furoic acid was the up-stream intermediate in route 1 and route 2, indicating that route 1 and route 2 were unlikely to be the oxidation route. In addition, the yield of 2-furoic acid was always less than 2% during all oxidation processes in our reaction system. Since MA was either determined to be in a very trace amount or was even undetectable using 2(5H)-furanone as the starting material, route 4 could be further excluded. Taking the above results into consideration, it was speculated that the oxidation reaction of furfural to MA over the P–C-600 catalyst proceeded *via* the path 3 oxidation route. Moreover, owing to their undersupplies and difficulty in the synthesis, Z-4-oxopent-2-enedial was not investigated in our study.

Conclusions

In the present study, an acid carbon catalyst doped with P was successfully synthesized using phytic acid, a naturally abundant biobased molecule, as the starting material. The synthesized P–C-600 catalyst demonstrated a superior catalytic activity in the catalytic oxidation of furfural to MA in an aqueous reaction system. A maximum MA yield of 76.3% was achieved at 60 °C for 10 h over P–C-600 in the presence of 8 equivalents of H_2O_2/furfural in the aqueous solution. The excellent catalytic performance of the P–C-600 catalyst should be ascribed to the high amount of Lewis acidic sites on the

catalyst surface. The as-synthesized P–C-600 catalyst exhibited a similar catalytic activity when being reused for up to four cycles. The P–C-600 catalyst could be a promising candidate in industrial-level applications for MA production in a green manner.

Conflicts of interest

There are no conflicts to declare.

Acknowledgements

References

1 H. Mandova, S. Leduc, C. Wang, E. Wetterlund, P. Patrizio, W. Gale and F. Kraxner, *Biomass Bioenergy*, 2018, **115**, 231–243.

2 V. P. Muiuane, M. Ferreira, P. Bignet, A. P. Bettencourt and P. Parpot, *J. Environ. Chem. Eng.*, 2013, **1**, 1237–1244.

3 Y. W. Tiong, C. L. Yap, S. Gan and W. S. P. Yap, *Ind. Eng. Chem. Res.*, 2018, **57**, 4749–4766.

4 Y. Luo, Z. Li, X. Li, X. Liu, J. Fan, J. H. Clark and C. Hu, *Catal. Today*, 2019, **319**, 14–24.

5 T. Deng, X. Cui, Y. Qi, Y. Wang, X. Hou and Y. Zhu, *Chem. Commun.*, 2012, **48**, 5494–5496.

6 S. Yamaguchi, M. Yabushita, M. Kim, J. Hirayama, K. Motokura, A. Fukuoka and K. Nakajima, *ACS Sustainable Chem. Eng.*, 2018, **6**, 8113–8117.

7 R. Wojcieszak, F. Santarelli, S. Paul, F. Dumeignil, F. Cavani and R. V. Gonçalves, *Sustainable Chem. Processes*, 2015, **3**, 9.

8 Y. Lou, S. Marinkovic, B. Estrine, W. Qiang and G. Enderlin, *ACS Omega*, 2020, **5**, 2561–2568.

9 T. Yang, W. Li, Q. Liu, M. Su, T. Zhang and J. Ma, *BioResources*, 2019, **14**, 5025–5044.

10 N. Alonso-Fagúndez, I. Agirrezabal-Telleria, P. L. Arias, J. L. G. Fierro, R. Mariscal and M. L. Granados, *RSC Adv.*, 2014, **4**, 54960–54972.

11 Y. Rodenas, R. Mariscal, J. L. G. Fierro, D. Martín Alonso, J. A. Dumesic and M. López Granados, *Green Chem.*, 2018, **20**, 2845–2856.

12 X. Li, B. Ho, D. S. W. Lim and Y. Zhang, *Green Chem.*, 2017, **19**, 914–918.

13 Y. Ni, Z. Bi, H. Su and L. Yan, *Green Chem.*, 2019, **21**, 1075–1079.

14 X. Li and Y. Zhang, *Green Chem.*, 2016, **18**, 643–647.

15 L. Chai, X. Hou, X. Cui, H. Li, N. Zhang, H. Zhang, C. Chen, Y. Wang and T. Deng, *Chem. Eng. J.*, 2020, **388**, 124187.

16 F. Menegazzo, E. Ghedini and M. Signoretto, *Molecules*, 2018, **23**, 2201.

17 S. Shi, H. Guo and G. Yin, *Catal. Commun.*, 2011, **12**, 731–733.

18 H. Guo and G. Yin, *J. Phys. Chem. C*, 2011, **115**, 17516–17522.

19 H. Choudhary, S. Nishimura and K. Ebitani, *Appl. Catal., A*, 2013, **458**, 55–62.

20 N. Alonso-Fagúndez, M. Ojeda, R. Mariscal, J. L. G. Fierro and M. López Granados, *J. Catal.*, 2017, **348**, 265–275.

21 J. Su, L. Yang, R. N. Liu and H. Lin, *Chin. J. Catal.*, 2014, **35**, 622–630.

22 T. Soták, M. Hronec, M. Gál, E. Dobročka and J. Škriniarová, *Catal. Lett.*, 2017, **147**, 2714–2723.

23 X. Li, B. Ho and Y. Zhang, *Ill. Nat. Hist. Surv., Biol. Notes*, 2016, **18**, 2976–2980.

24 H. Choudhary, S. Nishimura and K. Ebitani, *Chem. Lett.*, 2012, **23**, 409–411.

25 W. Zhu, F. Tao, S. Chen, M. Li, Y. Yang and G. Lv, *ACS Sustainable Chem. Eng.*, 2019, **7**, 296–305.

26 U. Thubsuang, S. Chotirut, K. Nuithitikul, A. Payaka, N. Manmuanpom, T. Chaisuwan and S. Wongkasemjit, *J. Colloid Interface Sci.*, 2020, **565**, 96–109.

27 C. Van Nguyen, J. R. Boo, C.-H. Liu, T. Ahamad, S. M. Alshehri, B. M. Matsagar and K. C. W. Wu, *Catal. Sci. Technol.*, 2020, **10**, 1498–1506.

28 X. Hu, M. Fan, Y. Zhu, Q. Zhu, Q. Song and Z. Dong, *Green Chem.*, 2019, **21**, 5274–5283.

29 C. Li, M. Yang, R. Liu, F. Zhao, H. Huang, Y. Liu and Z. Kang, *RSC Adv.*, 2014, **4**, 22419–22424.

30 Z. Long, L. Sun, W. Zhu, G. Chen, X. Wang and W. Sun, *Chem. Commun.*, 2018, **54**, 8991–8994.

31 M. A. Patel, F. Luo, M. R. Khoshi, E. Rabie, Q. Zhang, C. R. Flach, R. Mendelsohn, E. Garfunkel, M. Szostak and H. He, *ACS Nano*, 2016, **10**, 2305–2315.

32 J. Albero, A. Vidal, A. Migani, P. Concepcion, L. Blancafort and H. Garcia, *ACS Sustainable Chem. Eng.*, 2019, **7**, 838–846.

33 A. Villa, M. Schiavoni, P. F. Fulvio, S. M. Mahurin, S. Dai, R. T. Mayes, G. M. Veith and L. Prati, *J. Energy Chem.*, 2013, **22**, 305–311.

34 S. Campisi, F. Sanchez, D. Motta, T. Davies, N. Dimitratos and A. Villa, *C*, 2018, **4**, 9.

35 J. Datka, A. M. Turek, J. M. Jehng and I. E. Wachs, *J. Catal.*, 1992, **135**, 186–199.

36 E. Billeter, D. McGlamery, M. Aebli, L. Piveteau, M. V. Kovalenko and N. P. Stadie, *Chem. Mater.*, 2018, **30**, 4580–4589.

37 L. Zhou, Y. Sun, B. Li, Z. Li, Z. Zhang, J. Yun and R. Liu, *Catal. Commun.*, 2019, **126**, 44–49.

38 A. M. Puziy, O. I. Poddubnaya, M. Sobiesiak and B. Gawdzik, *Adsorption*, 2013, **19**, 717–722.

39 W. Li, S. Jin, R. Zhang, Y. Wei, J. Wang, S. Yang, H. Wang, M. Yang, Y. Liu, W. Qiao, L. Ling and M. Jin, *RSC Adv.*, 2020, **10**, 12908–12919.

40 Y. Wang, S. Zuo, J. Yang and S.-H. Yoon, *Langmuir*, 2017, **33**, 3112–3122.

41 X. Wu and L. R. Radovic, *Carbon*, 2006, **44**, 141–151.

42 L.-P. Yuan, Z.-Y. Wu, W.-J. Jiang, T. Tang, S. Niu and J.-S. Hu, *Nano Res.*, 2020, **13**, 1376–1382.

43 A. S. Singh, J. H. Advani and A. V. Biradar, *Dalton Trans.*, 2020, **49**, 7210–7217.

44 S. Kumar, M. B. Gawande, J. Kopp, S. Kment, R. S. Varma and R. Zbořil, *ChemSusChem*, 2020, **13**, 5231–5238.

45 H. Sato, *Catal. Rev.*, 1997, **39**, 395–424.

46 T. Mariappan, Y. Zhou, J. Hao and C. A. Wilkie, *Eur. Polym. J.*, 2013, **49**, 3171–3180.

47 H. Nakayama, T. Eguchi, N. Nakamura, S. Yamaguchi, M. Danjyo and M. Tsuhako, *J. Mater. Chem.*, 1997, **7**, 1063–1066.

48 A. MacIntosh, G. Jiang, P. Zamani, Z. Song, A. Riese, K. Harris, X. Fu, Z. Chen, X. Sun and G. Goward, *J. Phys. Chem. C*, 2018, **122**, 6593–6601.

49 L. Filiciotto, A. M. Balu, J. C. Van der Waal and R. Luque, *Catal. Today*, 2018, **302**, 2–15.

50 C. I. Meyer, A. J. Marchi, A. Monzon and T. F. Garetto, *Appl. Catal., A*, 2009, **367**, 122–129.

51 Y. Tachibana, T. Masuda, M. Funabashi, K.-I. Kasuya and M. Kunioka, *ACS Symp. Ser.*, 2012, **1105**, 91–110.

52 P. Kumar and R. K. Pandey, *Green Chem.*, 2000, **2**, 29–32.